Biochimica et Biophysica Acta 1838 (2014) 148–157

Contents lists available at ScienceDirect

Biochimica et Biophysica Acta

journal homepage: www.elsevier.com/locate/bbamem

Oxidative stress effect on progesterone-induced blocking factor (PIBF) binding to PIBF-receptor in lymphocytes

Carlos de la Haba [a,b], José R. Palacio [b], Tamas Palkovics [c], Júlia Szekeres-Barthó [c], Antoni Morros [a], Paz Martínez [b,*]

[a] Unitat de Biofísica, Departament de Bioquímica i de Biologia Molecular, Centre d'Estudis en Biofísica (CEB), Facultat de Medicina, Universitat Autònoma de Barcelona (UAB), 08193 Bellaterra, Barcelona, Spain
[b] Unitat d'Immunologia, Institut de Biotecnologia i de Biomedicina (IBB), Universitat Autònoma de Barcelona (UAB), 08193 Bellaterra, Barcelona, Spain
[c] Department of Medical Microbiology and Immunology, Medical School, Pécs University, Pécs, Hungary

ARTICLE INFO

Article history:
Received 15 May 2013
Received in revised form 23 July 2013
Accepted 8 August 2013
Available online 15 August 2013

Keywords:
Lymphocyte
PIBF-R
Oxidative stress
Membrane fluidity
Laurdan
Lipid raft

ABSTRACT

Receptor–ligand binding is an essential interaction for biological function. Oxidative stress can modify receptors and/or membrane lipid dynamics, thus altering cell physiological functions. The aim of this study is to analyze how oxidative stress may alter receptor–ligand binding and lipid domain distribution in the case of progesterone-induced blocking factor/progesterone-induced blocking factor-receptor. For membrane fluidity regionalization analysis of MEC-1 lymphocytes, two-photon microscopy was used in individual living cells. Lymphocytes were also double stained with AlexaFluor647/progesterone-induced blocking factor and Laurdan to evaluate -induced blocking factor/progesterone-induced blocking factor-receptor distribution in the different membrane domains, under oxidative stress. A new procedure has been developed which quantitatively analyzes the regionalization of a membrane receptor among the lipid domains of different fluidity in the plasma membrane. We have been able to establish a new tool which detects and evaluates lipid raft clustering from two-photon microscopy images of individual living cells. We show that binding of progesterone-induced blocking factor to progesterone-induced blocking factor-receptor causes a rigidification of plasma membrane which is related to an increase of lipid raft clustering. However, this clustering is inhibited under oxidative stress conditions. In conclusion, oxidative stress decreases membrane fluidity, impairs receptor–ligand binding and reduces lipid raft clustering.

1. Introduction

Progesterone-dependent immunomodulation is one of the mechanisms that enable pregnancy to proceed to term [1]. Immunologic effects of progesterone are mediated by a protein named progesterone-induced blocking factor (PIBF) which induces a Th2 cytokine production by T lymphocytes in vitro and in vivo and modulates peripheral NK activity. Though PIBF production is a characteristic feature of normal pregnancy, this molecule was recently found to be over-expressed in highly proliferating cells and malignant tumors independently from the progesterone receptor status [2,3].

PIBF binds to the glycosylphosphatidylinositol (GPI) anchored PIBF receptor (PIBF-R) which, upon ligand binding, combines with the alpha chain of the IL-4R for signaling. Therefore, engagement of the PIBF-R results in Jak1 phosphorylation which, in turn, activates STAT6 [1]. GPI-anchored proteins are enriched in the leukocyte membrane within glycosphingolipid-cholesterol rafts. These submicron domains need cholesterol for their function and, in line with this, depletion of cholesterol from the cell membrane abolished the STAT6 inducing effect of PIBF. In methyl-β-cyclodextrin (Mβ-CD) treated lymphocytes, neither PIBF nor IL-4 was able to Tyr-phosphorylate STAT6, suggesting that not only the PIBF-receptor but also the α chain of the IL-4 receptor might be raft-associated [4]. Lipid rafts are thought to be platforms within the plasma membrane which aid cell signaling and are rigid compared to other domains in the plasma membrane. These lipid rafts are enriched in sphingolipids and cholesterol and are associated to a subset of membrane proteins with an important role in signal transduction and membrane traffic [5–8].

Lipids within the plasma membrane are one of the preferential targets of reactive oxygen species (ROS) which cause lipid peroxidation. In particular, polyunsaturated phospholipids are an extremely vulnerable target, due to the susceptibility of their chains to lipid peroxidation [9,10]. Recent data have shown that oxidative stress, produced by ROS, can modify the receptors impairing their normal functions [11,12]. This process also disturbs the bilayer structure, modifies membrane properties such as membrane fluidity, alters the physiological functions of cell membranes

Abbreviations: DMSO, dimethylsulphoxide; FBS, fetal bovine serum; GP, generalized polarization; I_d, liquid disordered; I_o, liquid ordered; L_β, gel phase; PIBF, Progesterone-Induced Blocking Factor; PMA, phorbol-12-myristate-13-acetate; ROS, reactive oxygen species.

* Corresponding author. Tel.: +34 93 581 2804; fax: +34 93 581 2011.
E-mail address: Paz.Martinez@uab.es (P. Martínez).

0005-2736/$ – see front matter © 2013 Elsevier B.V. All rights reserved.
http://dx.doi.org/10.1016/j.bbamem.2013.08.006

and contributes to cell membrane damage [9,10]. Altered membrane fluidity might also affect membrane protein function by modifying lipid microenvironment and interactions [13–16]. Several reports have described a decrease of membrane fluidity in different cell membranes as a consequence of lipid peroxidation [17–20]. The immune system is composed by different cell types that have different sensitivities to oxidative damage, depending on their effector functions [20–24].

Recent techniques are able to visualize different lipid domains within the plasma membranes of individual cells [8,25,26]. One of these techniques, known as two-photon microscopy, allows obtaining high resolution images of single cells, in vivo, which enables visualizing the distribution of membrane fluidity in different domains within the plasma membrane. The environment-sensitive probe Laurdan (6-dodecanoyl-2-dimethylamino-naphthalene) is used, which exhibits an emission spectral maximum shift from 440 nm to 490 nm in the transition from gel phase to liquid phase [27,28]. By using a multiphoton confocal microscope it is possible to excite the fluorophore with two photons at double the wavelength causing it to fluoresce [27–33].

Previously we have reported that oxidative stress reduces plasma membrane fluidity of THP-1 induced macrophages [20]. Membrane rigidification may cause an impaired cellular function. In lymphocytes, PIBF-R signaling is essential for pregnancy; an inefficient receptor signaling could impair implantation. The aim of the present study is to analyze lymphocyte membrane fluidity and PIBF/PIBF-R binding distribution in different membrane lipid domains of individual cells, under oxidative stress conditions.

2. Materials and methods

2.1. Cell line culture

MEC-1 lymphocytes were established and characterized from peripheral blood of a patient with B-chronic lymphocytic leukemia [34]. MEC-1 cells were cultured in RPMI medium 1640, 10% fetal bovine serum (FBS) with GlutaMax and without phenol red (Invitrogen). Cells were maintained at 37 °C in 5% CO_2. All experiments were performed within the cell passages 20–50.

2.2. Analysis of cell viability under oxidative stress conditions

We determined the highest H_2O_2 concentration allowing acceptable levels of viability. 200 μl of MEC-1 lymphocytes at 5×10^6 cells/ml was seeded in each well of 96 microwell plates for viability analysis. Cells were then centrifuged at 300 ×*g* for 5 min and washed three times with PBS. H_2O_2 in fresh medium without FBS was added to final concentrations ranging from 0.1 mM to 10 mM. After 4 h at 37 °C and 5% CO_2 cells were centrifuged, washed and viability was assessed by MTT assay (EZ4U Cell Proliferation Assay, Biomedica Gruppe, Wein, Austria). This assay measures the reduction of MTT (3-[4,5-dimethylthiazol-2-yl]-2,5-diphenyltetrazolium bromide) to formazan (1-(4,5-dimethylthiazol-2-yl)-3,5-diphenylformazan) catalyzed by mitochondrial dehydrogenase in functional mitochondria. Results showed that the H_2O_2 concentrations below 5.0 mM for 4 h maintained cell viability above 80%.

2.3. Oxidative stress induction in MEC-1 cells for two-photon microscopy analysis

For oxidative stress induction, MEC-1 cells were centrifuged at 300 ×*g* for 5 min. Cell pellet was then resuspended in RPMI phenol and serum free medium at a final concentration of 10^6 cells/ml. Cells were then incubated during 2 h at 0.5, 1 or 2 mM H_2O_2 at 37 °C in a 5% CO_2 atmosphere. After oxidative induction, cells were washed three times with the same RPMI medium and thereafter cells were stained with Laurdan as described in section below.

2.4. Laurdan-staining of lymphocytes membranes

Lymphocytes were labeled with Laurdan (6-dodecanoyl-2-dimethylamino-naphthalene). Laurdan was dissolved to a concentration of 2 mM in dimethylsulfoxide (DMSO) and stored at −20 °C at the dark. For membrane labeling, cells were incubated in medium without FBS at a final concentration of 5 μM Laurdan for 30–60 min at 37 °C and 5% CO_2 with agitation. In the Laurdan-stained lymphocyte suspension the final concentration of DMSO was less than 0.25% (v/v). This cell suspension was used to evaluate membrane fluidity by two-photon microscopy.

2.5. Two-photon microscopy technique

Membrane fluidity distribution in stained lymphocytes was evaluated as previously described [20], with a multiphoton scanning confocal microscope Leica TCS-SP5 (Leica Microsystems, Heidelberg GmbH) at the Servei de Microscòpia (UAB). Images were obtained with a 63× oil immersion objective lens and a 1.4 numerical aperture, at a resolution of 512 × 512 pixels and at a scan speed of 400 Hz, by using LEICA LAS AF software. After fluorescence excitation with the multiphoton laser at 800 nm, the two-photon microscope captures two simultaneous emission images, with wavelengths ranging from 400–460 nm and 470–530 nm.

Emission intensities from every image pixel were introduced into the generalized polarization (GP) Eq. (1) providing a final GP value, which is a measure of membrane fluidity:

$$GP = \frac{I_{(400-460)} - G \times I_{(470-530)}}{I_{(400-460)} + G \times I_{(470-530)}} \quad (1)$$

where G is a correction factor for the microscope being used, which was calculated by using Eq. (2):

$$G = \frac{GP_{theo} + GP_{theo} \times GP_{exp} - 1 - GP_{exp}}{GP_{theo} \times GP_{exp} - GP_{theo} + GP_{exp} - 1} \quad (2)$$

where GP_{theo} is the GP theoretical value of a standard solution of 5 μM Laurdan in DMSO, which has a known value ($GP_{theo} = 0.207$), whereas GP_{exp} is the GP value of the same solution measured in our confocal microscope [35]. GP values range from −1, corresponding to the highest fluidity, to +1 for the lowest fluidity. GP images, therefore, show membrane fluidity distributions across the cell membrane providing an excellent tool for membrane dynamics visualization [20,36].

2.6. Image analysis

In order to obtain a GP value for each pixel, a WiT 8.3 imaging software (Dalsa Digital Imaging, Canada) was used and adapted for two-photon images. All calculations were carried out in floating point format and all images were first converted to 8-bit unsigned format [36]. Images were then processed with a custom made sub-program. Background values were set to zero: Eq. (1) denominator was converted to a binary image with background values set to zero and nonbackground values set to one, then the binary image was multiplied by the GP image [32]. Images were then pseudo colored by means of Adobe Photoshop 7.0. All GP images were corrected using the G factor previously obtained from a 5 μM Laurdan solution for each experiment [36]. GP distributions were obtained from the histograms of the GP images.

2.7. Detection of PIBF receptors in lymphocytes by conventional confocal microscopy

MEC-1 lymphocytes were first placed under oxidative stress as described above. After the 2 h incubation with hydrogen peroxide, cells were washed and incubated with soluble PIBF bound to AlexaFluor647 fluorochrome. Fifty microliters of PIBF-AlexaFluor647,

at a concentration of 25 μg/ml, was added to 2×10^6 cells and incubated for 1 h at 37 °C. Then cells were washed three times and stained with Laurdan as described in section above. PIBF receptor images were obtained with a conventional confocal microscope Leica TCS-SP5 (Leica Microsystems, Heidelberg GmbH), at the Servei de Microscòpia (UAB) consecutively after obtaining membrane fluidity images.

2.8. Assessment of lipid peroxidation in lymphocyte membranes

Lipid peroxidation in lymphocyte membranes was assessed, as previously described [20], by using C11-BODIPY$^{581/591}$ (4,4-difluoro-5-(4-phenyl-1,3-butadienyl)-4-bora-3a,4a-diaza-s-indacene-3-undecanoic acid, Invitrogen), a fluorescent fatty acid analog which incorporates into membranes. Upon oxidation, both the excitation and emission fluorescence spectra of the dye shift to shorter wavelengths [37,38]. A 2 mM stock solution of C11-BODIPY$^{581/591}$ was prepared by dissolving the probe in DMSO and then it was stored at −20 °C in the dark.

200 μl of MEC-1 lymphocytes at 1×10^6 cells/ml was seeded in each well of 96-microwell plates for probe incorporation. Cells were then centrifuged and washed three times with PBS and stained in medium without FBS at a final concentration of 10 μM C11-BODIPY$^{581/591}$ for 45 min at 37 °C and 5% CO_2. After BODIPY incubation, cells were centrifuged and washed three times with PBS. H_2O_2 was then added to a final concentration ranging from 0.25 mM to 5 mM, and cells were incubated for 2 h at 37 °C. Control cells were incubated in the same conditions without H_2O_2. A multi-well spectrofluorometer (Victor3, Perkin-Elmer) was used to measure the emissions corresponding to the oxidized (green fluorescence: $\lambda_{excitation}$, 488 nm; $\lambda_{emission}$, 520 nm) and non-oxidized (red fluorescence: $\lambda_{excitation}$, 545 nm; $\lambda_{emission}$, 590 nm) states of the probe. Oxidation of C11-BODIPY$^{581/591}$ was estimated by calculating the ratio between green fluorescence (oxidized) and total fluorescence (oxidized plus non-oxidized), in order to normalize for probe uptake and distribution into cellular membranes [39].

Lipid peroxidation induced by hydrogen peroxide was compared to the effect of the free radical initiator 2,2′-azobis(2-amidinopropane) dihydrochloride (AAPH) (Sigma-Aldrich). AAPH has been used successfully to study the actions of free radicals upon cell membrane lipid peroxidation [38,40,41]. To assess the azo compound oxidizing effect, 5 mM AAPH solution in medium without FBS was added to lymphocytes loaded with C11-BODIPY$^{581/591}$, as described above, in 96-well plates. The plates were incubated for 2 h at 37 °C. Oxidation of C11-BODIPY$^{581/591}$ was estimated by calculating the ratio between green fluorescence and total fluorescence.

2.9. Statistics

Statistical analyses were performed by using SigmaPlot for Windows 11.0 (Systat Software, Inc.). The number of cells analyzed (n) for each experiment ranged from 100 to 200. Comparisons between control and oxidation treatments were performed by one-way analysis of variance based on ranks (Kruskal–Wallis) followed by post-hoc Dunn's test. Statistical significance was set at $p < 0.05$.

3. Results

3.1. Lymphocyte membrane fluidity distribution under oxidative stress in single cells by two-photon microscopy

GP images and GP frequency distribution graphs show that lymphocytes under oxidative stress become substantially enriched in high GP areas orange–red colored, corresponding to rigid domains. Fig. 1(A–D) shows the Laurdan generalized polarization (GP) images of MEC-1 cells, at 37 °C, in control conditions (Fig. 1A) and in oxidizing conditions, in 0.5 mM H_2O_2 (B), 1 mM H_2O_2 (C) and 2 mM H_2O_2 (Fig. 1D). Images (Fig. 1A–D) were pseudocolored with an arbitrary color palette (Fig. 1D), which shows extreme fluidity (GP value −1) in purple color and extreme rigidity (GP value +1) in red color.

GP images were then transformed to GP frequency distributions curves for quantification of membrane fluidity differences. GP frequency distributions, at 37 °C, of control and treated lymphocytes are shown in Fig. 1F. For a better observation of these frequency changes, GP frequency distribution values of control cells were subtracted from the corresponding values of each GP distribution of H_2O_2 treated lymphocytes (Fig. 1F). The resulting frequency difference curves are shown in Fig. 1G. Oxidation increases the frequency difference in GP values from +0.30 to +1.00, whereas GP values from −0.5 to +0.3 decrease in frequency. In order to statistically analyze the frequency changes for every single cell, the area under the frequency distribution curve (Fig. 1F) of these two GP zones was measured and compared. The results of this analysis showed that higher GP values, from +0.30 to +1.00, in treated cells showed a significant increase ($p < 0.05$) compared to control cells (data not shown). This increase was at the expense of a significant

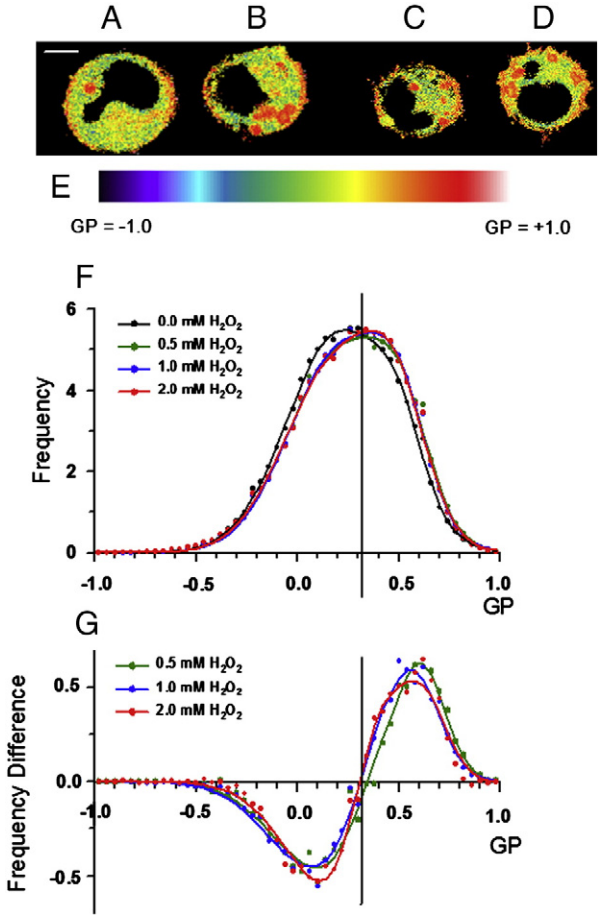

Fig. 1. GP images and GP frequency distributions Laurdan-stained lymphocytes under oxidative stress. MEC-1 lymphocytes were incubated without H_2O_2, as control cells, (A) and with: 0.5 mM H_2O_2 (B), 1 mM H_2O_2 (C) and 2 mM H_2O_2 (D) for 2 h. Scale bar, 5 μm. After incubation, lymphocytes were stained with 5 μM Laurdan. Images were collected (n = 100) at 37 °C in a two-photon microscope, GP images were calculated and then pseudocolored with an arbitrary color palette (E). GP images were transformed to GP frequency distribution curves and normalized (sum = 100) (F): dots show experimental data and continuous lines show best fitting curves to the experimental data using the Gaussian functions or Weibull functions for asymmetric curves. GP frequency distribution values of control lymphocytes were subtracted from the corresponding values of each GP distribution of H_2O_2 treated lymphocytes. The resulting frequency difference distribution curves are shown in (G): dots indicate values of the resulting frequency differences and smoothed lines were obtained using a Savitzky–Golay algorithm. A vertical line has been drawn in F and G diagrams, crossing the GP point with common frequencies (GP ~ +0.3), to help defining two zones with different behavior in the GP scale.

decrease of the intermediate GP values (from −0.5 to +0.3). This suggests that, as a consequence of oxidation, lymphocyte plasma membrane becomes more rigid.

It is interesting to attribute the above described GP frequency changes to the different kinds of lipid phases, as it is accepted for lipid bilayers of viable cell membranes. The GP values corresponding to these different lipid phases have been estimated by comparison with membrane models showing compositions similar to those of cell membranes [36,42,43]. GP values above +0.55 and below −0.05 represent membranes in gel and fluid phases, respectively [36,42]. GP values approximately between +0.25 and +0.55 have been attributed to liquid-ordered (l_o) or lipid raft domains whereas GP values between −0.05 and +0.25 would correspond to the surrounding non-raft regions or liquid-disordered (l_d) phase [5,29].

An increase in the frequency of a given GP population, observed for oxidized lymphocytes in Fig. 1F–G, may be interpreted as: 1) an increase in the corresponding mean domain size, through domain clustering and/or 2) an increase in the abundance of this kind of domains, as suggested by Gaus et al. [36]. Two-photon microscopy allows visualizing the distribution of lipid domains, so that an accurate quantification of the size and the number of every type of domains can be obtained from the original experimental data. Therefore we investigated if raft domains, as platforms for efficient signaling, could increase in number or in size. These two parameters were statistically analyzed from the data obtained for every single cell, as previously described [20], by using a custom-made software. The mean and SEM obtained for the size of domains with +0.25 > GP < +0.55 (lipid rafts) and for the size of domains with GP > +0.55 (gel phase), for control or oxidized lymphocytes are shown in Fig. 2. No significant changes were found in the size of raft domains or in the size of gel-like domains as a consequence of H_2O_2 lymphocyte oxidation (Fig. 2A). However, the number of both lipid raft and gel-like domains significantly increased as the H_2O_2 concentration raised (Fig. 2B).

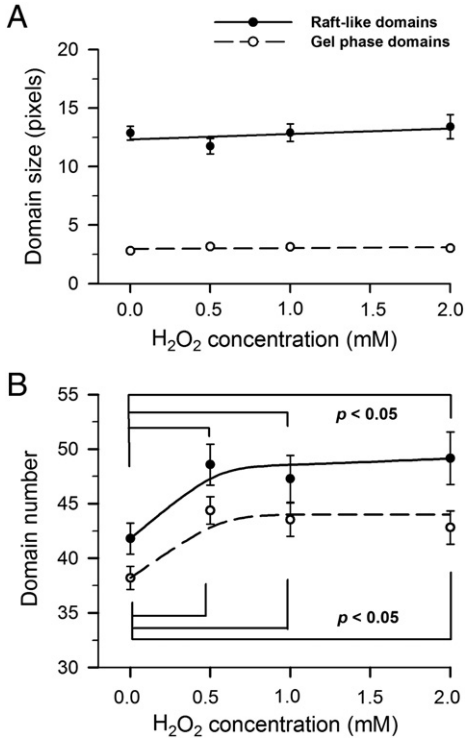

Fig. 2. Statistical analysis of the size and the number of rigid membrane domains. The mean size, in pixels, (A) and the mean domain number (B) of the raft (+0.25 < GP < +0.55) and gel phase domains (GP > +0.55) were plotted as a function of hydrogen peroxide concentration. Error bars correspond to SEM. Statistical analysis showed significant differences ($p < 0.05$) between control and treated lymphocytes in the mean domain number of both raft and gel phase domains.

3.2. PIBF/PIBF-R binding and membrane dynamics in lymphocytes

For the study of PIBF binding to its receptor, conventional confocal microscopy and two-photon microscopy were used. Lymphocytes were double stained with AlexaFluor647/PIBF and Laurdan. The excitation and emission wavelengths patterns of these fluorochromes are suitable to yield separate information without interference. PIBF fluorescence images were obtained by conventional microscopy and GP images by two-photon microscopy; both images were consecutively acquired for comparison. Information of PIBF distribution in the different kinds of membrane domains was determined by superposition of GP images to their corresponding PIBF fluorescent images. For two-photon microscopy, lymphocytes were incubated with recombinant PIBF for 1 h and membrane fluidity distribution evaluated by two-photon microscopy. The GP images (Fig. 3A–C) show an enrichment of high GP areas orange–red colored in the lymphocyte surface, corresponding to rigid regions, due to binding of PIBF to its receptor. GP frequency distributions, at 37 °C, of control and PIBF bound lymphocytes, which presented interesting differences when compared, are shown in Fig. 3D. A vertical line has been drawn in Fig. 3D crossing the GP point with common frequencies (GP ~ +0.3), to help defining two zones with different behavior in the GP scale. For a better observation of these frequency changes, GP frequency distribution values of control lymphocytes were subtracted from the corresponding values of each GP distribution of activated lymphocytes (Fig. 3D). The resulting frequency difference curves are shown in Fig. 3E where the two above defined GP zones can also been observed. This figure shows that PIBF binding induces a curve shift towards the high positive end of the GP scale. GP values of PIBF bound lymphocytes from −0.5 to +0.3 decrease in frequency while GP values from +0.3 to +1.00 increase in frequency. These results show that plasma membranes of lymphocytes bound to PIBF become more rigid than non bound plasma membranes.

Results showed that lipid raft domains significantly increase in size when PIBF binding occurs (Fig. 4A). The mean number (Fig. 4B) of lipid raft domains significantly decreases upon PIBF binding. With this procedure we have an evidence that PIBF binding in lymphocytes causes clustering of lipid raft and gel-like domains.

3.3. Effect of oxidative stress on PIBF/PIBF-R binding and membrane fluidity in lymphocytes

In H_2O_2-treated cells there is a substantial loss of high end positive GP pixels, colored in orange–red, on the lymphocyte surface. Fig. 5A–E shows the Laurdan generalized polarization (GP) images of PIBF bound MEC-1 cells, at 37 °C, in control conditions (0.0 mM H_2O_2) (A) and in oxidizing conditions from 0.5 to 2.0 mM H_2O_2 (B–D). GP frequency distributions, at 37 °C, of control and treated lymphocytes are shown in Fig. 5F and the resulting subtracted frequency difference curves are shown in Fig. 5G. Frequency distribution curves (Fig. 5F–G) show that oxidation induces a decrease of frequency in GP values from +0.30 to +1.00, whereas GP values from −0.5 to +0.3 increase in frequency. These results show that plasma membranes of lymphocytes bound to PIBF under oxidative stress become more fluid than the membranes of non-oxidized cells.

Lipid domain analysis of lymphocytes in the presence of PIBF, under oxidative stress, showed a decrease of lipid raft clustering. The average raft size of PIBF bound to its receptor in lymphocytes was reduced significantly by 2 mM H_2O_2 (Fig. 6). Although the results for raft size were not significantly different at 0.5 and 1.0 mM, as compared to the control, a concentration dependent decrease tendency can be observed. Raft domain number and gel-like domain number did not vary significantly under oxidative conditions.

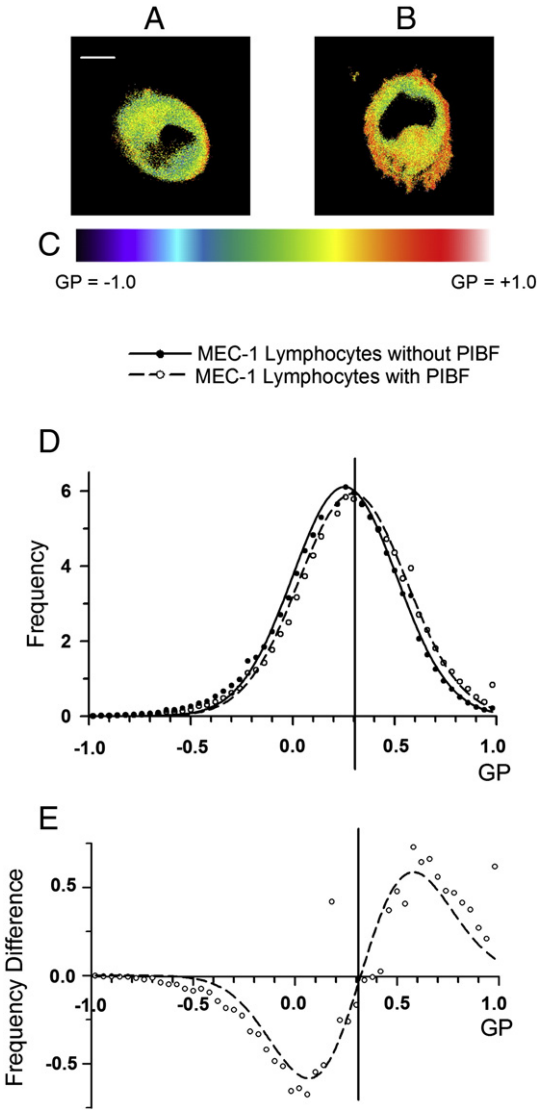

Fig. 3. Effect of PIBF/PIBF-R on lymphocyte plasma membrane fluidity. MEC-1 lymphocytes were incubated without PIBF as control cells (A) and with 25 μg/ml sPIBF (B) for 1 h at 37 °C. Scale bar, 5 μm. After incubation, lymphocytes were stained with 5 μM Laurdan. Images were collected (n = 100) at 37 °C in a two-photon microscope. GP images were calculated and then pseudocolored with an arbitrary color palette (C). GP images were transformed to GP frequency distribution curves and normalized (sum = 100) (D): dots show experimental data and continuous lines show best fitting curves to the experimental data using the Gaussian functions or Weibull functions for asymmetric curves. GP frequency distribution values of control lymphocytes were subtracted from the corresponding values of each GP distribution of PIBF bound lymphocytes. The resulting frequency difference distribution curves are shown in (E): dots show experimental values of the resulting frequency differences and smoothed lines were obtained using a Savitzky–Golay algorithm. A vertical line has been drawn in D and E diagrams, crossing the GP point with common frequencies (GP ~ +0.3), to help defining two zones with different behavior in the GP scale.

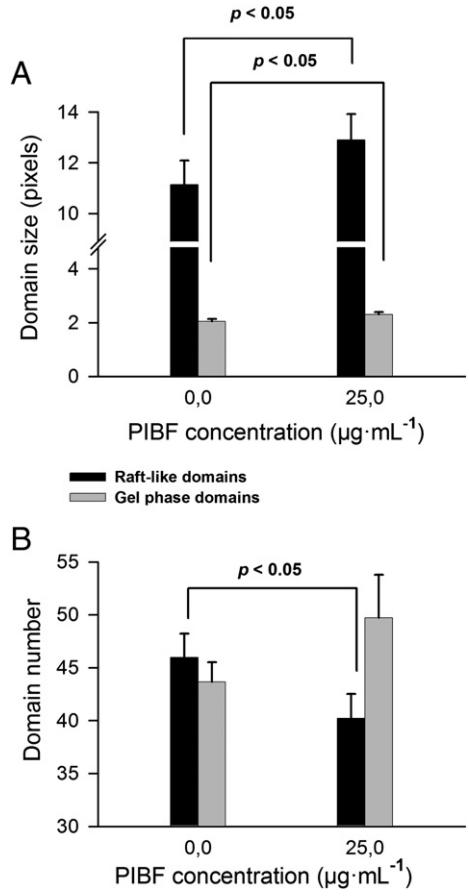

Fig. 4. Statistical analysis of the size and the number of rigid membrane domains induced by PIBF/PIBF-R binding. The mean size, in pixels, (A) and the mean domain number (B) of the raft (+0.25 < GP < +0.55) and gel phase domains (GP > +0.55) were plotted for control and PIBF bound lymphocytes. Error bars correspond to SEM. Statistical analysis showed significant differences ($p < 0.05$) between PIBF bound lymphocytes and control cells in the size of both lipid raft and gel phase domains, and in the number of lipid raft domains.

3.4. PIBF/PIBF-R membrane distribution in lymphocytes under oxidative stress

PIBF binding to its receptor was evaluated by conventional confocal microscopy. Lymphocytes were placed under oxidative stress and incubated with PIBF-AlexaFluor647 for 1 h. Fig. 7C shows the fluorescence intensity values of PIBF bound to its receptor as a function of H_2O_2 concentration. These results show that lymphocytes under oxidative stress have less fluorescence intensity of PIBF/PIBF-R binding, indicating that less binding is achieved.

Taking advantage of the double staining approach, we obtained total PIBF intensities which corresponded to each phase of the lipid membrane. We matched the PIBF fluorescence intensity of each pixel with their corresponding pixel in the GP image. We grouped all the PIBF fluorescent pixels in the different membrane phases using their corresponding GP value: fluid phase (GP < −0.05), non-raft (−0.05 < GP < 0.25), lipid raft (+0.25 < GP < 0.55) and gel phase (GP > 0.55). The intensities of the pixels were added in each group. This analysis was performed under oxidative stress conditions. Results are shown in Fig. 7D. Control lymphocytes bound to PIBF, without oxidative stress, had higher fluorescence intensity in all the phases compared to lymphocytes under oxidative stress. The fluorescence intensity upon PIBF binding decreased under oxidative stress conditions: around 20% in the fluid phase, 30% in the non-raft, 40% in the lipid raft and 50% in the gel phase.

3.5. Lipid peroxidation in lymphocytes under oxidative stress conditions

For a better understanding of the molecular mechanisms involved in oxidative stress and changes in membrane dynamics, membrane lipid peroxidation was determined in our experimental conditions. Oxidation of the probe C11-BODIPY581/591 showed significant levels of lipid peroxidation at 2 and 5 mM H_2O_2 concentrations. Lipid peroxidation is prevented by the antioxidative activity of the cell at low H_2O_2 concentrations. The positive control, a free radical initiator AAPH (Fig. 8), also showed significant high levels of lipid peroxidation.

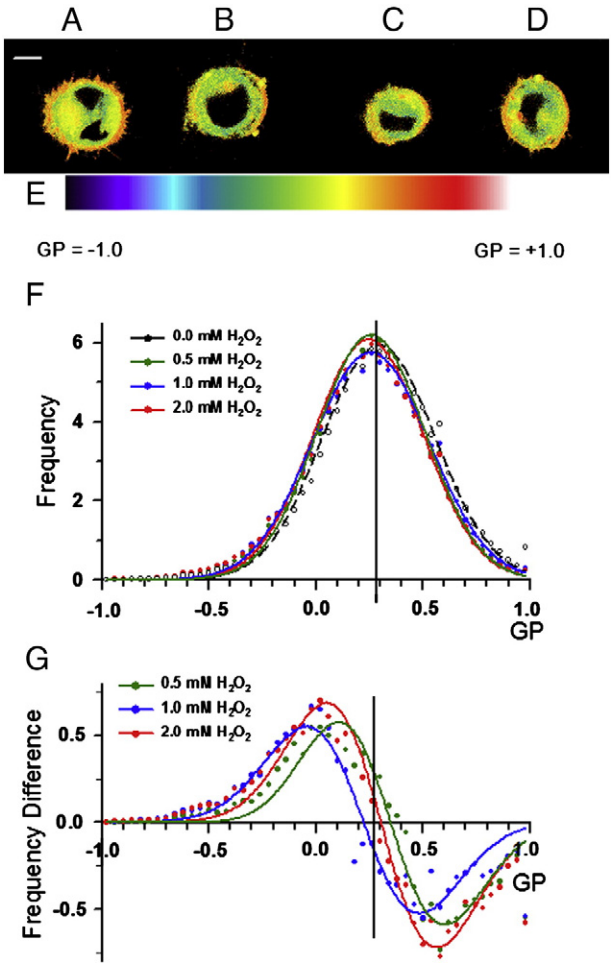

Fig. 5. Membrane fluidity distribution in PIBF bound lymphocytes under oxidative stress. MEC-1 lymphocytes were incubated without H_2O_2, as control cells, (A) and with: 0.5 mM H_2O_2 (B), 1 mM H_2O_2 (C) and 2 mM H_2O_2 (D) for 2 h. Scale bar, 5 μm. After incubation all lymphocytes, including control cells, were activated with 25 μg/ml sPIBF at 37 °C for 1 h. Then cells were stained with 5 μM Laurdan. Images were collected (n = 150) at 37 °C in a two-photon microscope. GP images were calculated and then pseudocolored with an arbitrary color palette (E). GP images were transformed to GP frequency distribution curves and normalized (sum = 100) (F): dots show experimental values and continuous lines show best fitting curves to the experimental data using the Gaussian functions or Weibull functions for asymmetric curves. GP frequency distribution values of control lymphocytes were subtracted from the corresponding values of each GP distribution of H_2O_2 treated lymphocytes. The resulting frequency difference distribution curves are shown in (G): dots indicate values of the resulting frequency differences and smoothed lines were obtained using a Savitzky–Golay algorithm. A vertical line has been drawn in F and in G diagrams to help defining two zones with different behavior in the GP scale.

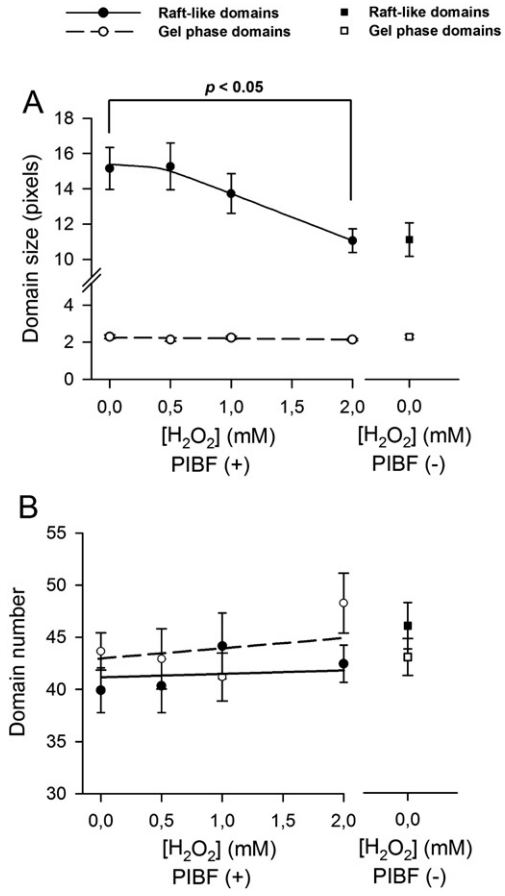

Fig. 6. Statistical analysis of the size and the number of rigid membrane domains in PIBF bound lymphocytes under oxidative stress conditions. The mean size, in pixels, (A) and the mean domain number (B) of the raft (+0.25 < GP < +0.55) and gel phase domains (GP > +0.55) were plotted for PIBF bound lymphocytes and control cells. Error bars correspond to SEM. Oxidative stress by 2.0 mM H_2O_2 induced significant differences ($p < 0.05$) for raft domain size in PIBF bound lymphocytes.

4. Discussion

We used a high resolution technique, two-photon microscopy, which allows visualizing individual living cells. This allows obtaining important biological results on viable cells without altering the properties of the plasma membrane. The aim was to analyze the effects of oxidative conditions on lymphocyte membrane fluidity regionalization, i.e. distinguishing lipid macrodomains in the plasma membrane.

The membrane fluidity distribution obtained for non oxidized lymphocytes in the present study showed GP frequency values similar to those obtained with lymphocytes in similar conditions by Gaus et al. [5]. Interesting results were obtained in our group: lymphocyte membrane fluidity distribution curve was shifted towards higher GP values when compared to macrophage membrane fluidity distribution [20] suggesting a more rigid membrane in lymphocytes as compared to macrophages. This is in accordance with the function of these two types of cells. It has also been described [32] that aortic endothelial cells have a GP distribution similar to our lymphocyte GP data.

Under oxidative stress conditions, lymphocytes underwent a significant increase in frequency of both rigid lipid domains: lipid rafts and gel phase domains. Previously we have described a significant increase in frequency of both rigid lipid domains of macrophage membranes under oxidative stress [20] which is consistent with the data presented in this article. Although oxidative stress has been extensively studied, no previous data in the literature have been reported by using two-photon microscopy.

The increase observed in lipid raft frequencies in oxidized lymphocytes can be attributed either to an increase in mean domain size, mediated by domain clustering, or to an increase in the number of this kind of domains, as suggested by Gaus et al. [36]. It is presently accepted that, in unstimulated cells, lipid rafts appear as small in size (under 250–300 nm) and unstable domains. Nevertheless, in several cellular biological functions, these small domains fuse giving rise to larger, stable, biologically active lipid rafts. Therefore we applied a novel computer software, previously developed in our group [20], for the analysis of the size and number of lipid rafts. This new tool allowed determining that the increase in rigidity of lymphocyte membranes under oxidative stress was due to an increase in number, rather than in size, of rigid domains. These results obtained in lymphocytes are in line with our earlier results on macrophages where increased number, but not size, of raft and gel-like domains was also observed due to oxidative stress [20]. In studies using detergent-resistant membrane (DRM) from endothelial

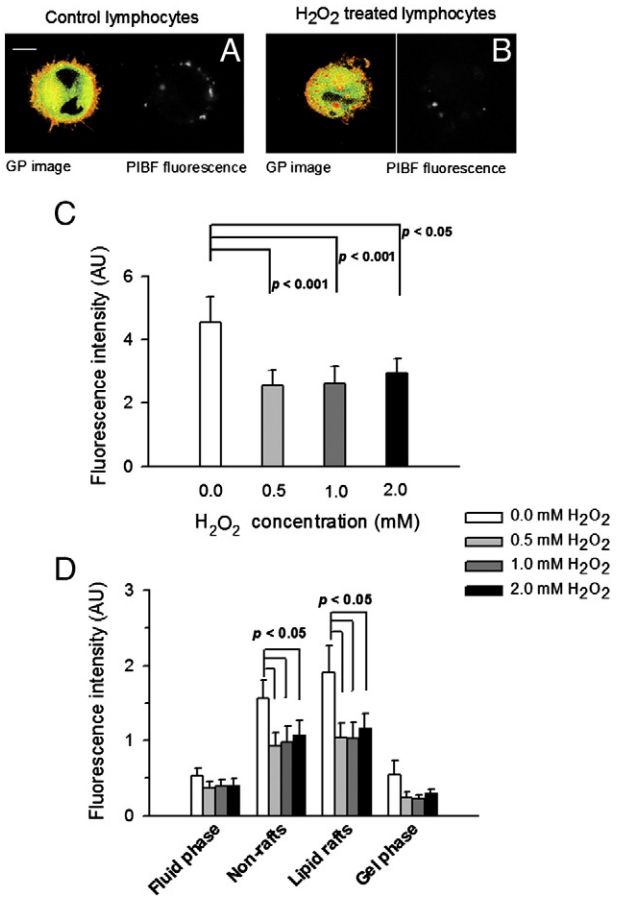

Fig. 7. PIBF/PIBF-R binding distribution in lymphocytes under oxidative stress conditions. MEC-1 lymphocytes were incubated without H_2O_2, as control cells, and with: 0.5 mM H_2O_2, 1 mM H_2O_2 and 2 mM H_2O_2 for 2 h. Scale bar, 5 μm. After incubation all lymphocytes, including control cells, were activated with 25 μg/ml sPIBF at 37 °C for 1 h. Then cells were stained with 5 μM Laurdan. This figure shows GP and PIBF fluorescence images of representative PIBF bound lymphocytes in the absence (A) and in the presence (B) of 2 mM H_2O_2. Scale bar, 5 μm. PIBF fluorescence images were collected (n = 160 cells) at 37 °C in a conventional confocal microscope. The PIBF fluorescence of whole cells was analyzed at each H_2O_2 concentration (C) and significant differences ($p < 0.05$ or $p < 0.001$) were found as compared to the control. PIBF/PIBF-R binding distribution was analyzed and compared among the different kinds of domains in plasma membrane under oxidative stress (D). In all H_2O_2 concentrations, significant differences ($p < 0.05$) were found in raft and non-raft PIBF distribution when compared to lymphocytes in the absence of H_2O_2.

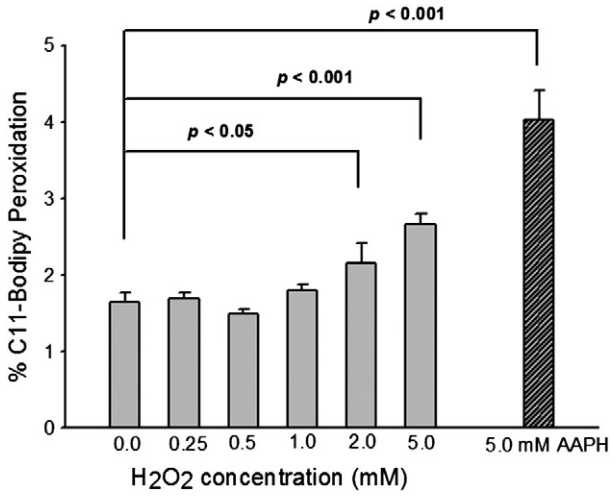

Fig. 8. Lymphocyte membrane lipid peroxidation under oxidative stress. MEC-1 lymphocytes were stained with the lipid analog C11-BODIPY$^{581/591}$ treated with H_2O_2 for 2 h at 37 °C. Bars indicate the mean percentage values of C11-BODIPY oxidation. Error bars correspond to SEM. Statistical analysis showed significant differences between oxidized lymphocytes and control ($p < 0.05$) for 2.0 mM H_2O_2 and ($p < 0.001$) for 5.0 mM H_2O_2. 5.0 mM azo initiator (AAPH) was used as a positive lipid peroxidation control.

cells, it has been reported an increase of lipid rafts as a response to oxidative stress which may lead the cell towards a survival or apoptotic pathway [20,44,45]. The implication of ROS in lipid raft formation in the plasma membrane of other types of cells has previously been described by using raft isolation and visualization techniques [44,46]. Several studies have also reported an increase of lipid rafts in membrane extracts of lymphocytes [47] and other cell lines [44], under oxidative stress conditions.

Most of the literature is concentrated in lipid rafts, although gel-like domains are also present in the plasma membrane. In biological membranes, the size of the lipid domains, as lipid rafts or gel-like domains, depends on the complexity of the membrane lipid composition, lipid–lipid interactions and on the presence of multivalent lipid-binding proteins [48]. Other factors like the membrane-associated cytoskeleton would play a major role both in regulating raft size [49] and in lateral domain positioning. Also in model membranes the domain formation, size, and shape, critically depend on various experimental conditions [42].

Changes in membrane fluidity could affect cell function through receptor–ligand binding. We used MEC-1 lymphocytes to investigate PIBF binding to its receptor (PIBF-R) in lymphocytes under physiological or oxidative stress conditions. Upon PIBF binding to its receptor in physiological conditions, the membrane of lymphocytes became enriched in rigid domains. This increase of rigid domains caused by receptor–ligand interactions in T-lymphocyte membranes after the interaction of CD3 with anti-CD3-coated polystyrene beads was also described by Gaus et al. [5], or in detergent-resistant membrane (DRM) extracts from T-lymphocytes activated with anti-CD3 by Larbi et al. [50]. This rigidification process has also been observed in cell to cell interactions: Gaus et al. [5] observed a frequency increase in high GP values at the site of formation of the immunological synapse in studies with T lymphocytes and dendritic cells. All these reports together suggest that changes in membrane fluidity are a key feature in many important membrane biological functions.

Surprisingly, although membrane fluidity distribution showed similar results for PIBF bound to lymphocytes and for lymphocytes placed under oxidative stress, the domain analysis revealed important differences in domain size and number. While lymphocytes under oxidative stress increased the number of small lipid raft domains and no clustering was detected, in case of PIBF/PIBF-R binding, raft domains within the plasma membrane were clustering together forming large raft platforms. This would trigger different biological responses through signal transduction pathways. It is reported in the literature that upon stimulation, e.g., ligand–receptor binding, the raft-preferring receptors tend to cluster, inducing large stabilized lipid rafts, from small unstable rafts [6,51,52]. Reports have described, using DRMs, raft clustering upon activation of the Fcγ receptor IIA (FcγRIIA) in U937 monocytes [53]. Altrock et al., by using conventional confocal microscopy, reported raft clustering upon interaction of integrins to a fibronectin layer in human acute myelogenous leukemia KG-1 myeloblasts [54]. In isolated DRM from B cells, raft coalescence has been described [55]. The formation of larger rafts is thought to aid cell signaling. In conclusion, the detailed analysis of rafts is required as a complementary study to better understand the biological significance of raft dynamics within cell function.

In the present study (Fig. 6A) raft-like domains in control lymphocyte membranes appear to be bigger than gel phase domains. In a previous report [20] we found in macrophages that raft-like domains have a double mean size as compared with gel-like domains. A similar result was obtained by Goñi & Alonso [56] in model membranes.

We propose that gel-like domains observed in our studies could correspond, as indicated by their high GP values, at least partially to ceramide (Cer) enriched domains. These kinds of rigid domains have been shown to be present in cellular membranes and they are involved in cell processes [57]. The molecular functions and Cer-enriched membrane platforms seem to be the reorganization of receptor and intracellular signaling molecules [58]. It has been proposed that, in complex systems like plasma membranes, gel-like Cer-enriched domains do not appear to exist as large platforms but, instead, they appear as small "islands" of L_β phase [56]. As stated by Silva et al., Cer per se is not able to induce neither the formation of large platforms in model membranes nor domain coalescence [59]. On the contrary, the formation of large gel-like platforms has been associated with cell apoptosis and other pathological conditions [58,60]. Interestingly, in our experimental conditions gel-like domains appear small in size; cells are alive with a viability above 80%.

Our focus of interest is to establish a relationship between oxidative stress and lipid peroxidation, membrane fluidity and plasma membrane receptor–ligand interactions. Our model was the binding of PIBF to its receptor in lymphocytes. Conventional confocal microscopy revealed decreased PIBF receptor–ligand binding under oxidative stress, as compared to control lymphocytes. This could be attributed either to oxidative modifications on the receptor or to the lipid dynamics of plasma membrane.

Several data reported cellular impaired functions under oxidative conditions. Denu and Tanner have shown how these conditions are able to inactivate protein phosphatases in vitro [61]. Other studies showed that the Epidermal Growth Factor (EGF) receptor in A549 adenocarcinoma cells becomes aberrantly phosphorylated in comparison of the control cells [11]. It has also been reported in an osteoblastic cell line (OB-6) a decreased cellular signaling and a decreased cellular protein expression of the Wnt signaling pathway [12]. This is consistent with our results of PIBF binding in which the efficiency of signal transduction through the receptor could be then diminished.

We compared lymphocytes in the absence of PIBF in control conditions to lymphocytes bound to PIBF under oxidative stress conditions. Two-photon microscopy and domain analysis showed interesting results. Our two-photon data showed a drastic decrease in the frequency of lipid rafts in the PIBF bound lymphocyte membranes: their fluidity distribution is nearly coincident with that of lymphocytes in resting conditions (and in the absence of PIBF). This indicates that the rigidifying changes in membrane fluidity induced by PIBF binding in untreated cells are abolished by oxidative stress. These results again confirm how oxidative stress perturbs drastically membrane dynamic changes induced by PIBF/PIBF-R binding.

Domain analysis of lymphocytes in the presence of PIBF revealed that oxidative stress caused a drastic decrease in lipid raft size in such a way that the size is at the same order as resting lymphocytes. Our results demonstrate that oxidative stress produces modifications in the plasma membrane lipid domain dynamics which can account for the reduced receptor–ligand interaction. These oxidative membrane modifications would induce an effect on the receptor structure and binding.

Interestingly, at high levels of oxidative stress conditions, two simultaneous significant changes were observed: lipid peroxidation and inhibition of lipid raft clustering. This suggests that oxidative stress modifies phospholipids within the plasma membrane, thus altering the physical properties and dynamics of the membrane. All these modifications can inhibit raft clustering and finally alter receptor–ligand interactions.

Under normal pregnancy conditions the concentration of PIBF continuously increases during gestation. Check et al. [62] reported that the failure to detect PIBF at 3–5 weeks of seemingly normal pregnancies is associated with a higher miscarriage rate. PIBF induces Th2 dominant cytokine production by progesterone receptor-positive pregnancy lymphocytes [63–65], a required feature of normal human pregnancy. It was also reported by Kelemen et al. [66] that PIBF induces increased production of asymmetric antibodies during pregnancy. Therefore, PIBF was proposed as a progesterone-induced immunomodulatory molecule secreted by lymphocytes, mainly uterine or decidual γδ T cells, during pregnancy [1].

The decreased PIBF binding caused by oxidative stress occurred mainly in lipid raft domains. This kind of domains acts as platforms which aid cell signaling. PIBF receptor has been shown to be raft-associated [67], therefore a disruption of raft clustering under oxidative conditions could directly affect cell signaling [52]. PIBF/PIBF-R binding in lymphocytes has been shown to induce IL-3, IL-4 and IL-10, through the STAT6 signaling pathway [1]. Recent studies have shown that increased expression of pro-inflammatory cytokines and low levels of PIBF and IL-10 are associated to preterm delivery [68].

Progesterone causes a release of PIBF which modulates the anti-abortive effect of progesterone. Patients with spontaneous abortions have been shown to have low PIBF (50%) and IL-10 levels [68]. Our PIBF results with conventional confocal microscopy show a reduced binding (40%) of PIBF to its receptor and lipid dynamic modifications due to oxidative stress. This could be a risk factor for spontaneous abortion caused by oxidative stress related pathologies.

Kozma et al. [4] demonstrated an association of the PIBF receptor and IL-4Rα. The binding ligand–receptor activates the STAT6 pathway mediated by IL-4Rα. A decrease in PIBF concentration or in the binding efficiency of this molecule to its receptor, or even an inhibition of the cocapping of PIBF and IL-4R would partially or totally suppress the intracellular signaling pathways giving a cytokine profile not compatible with gestation.

It is clear the great importance of the binding PIBF/PIBF-R for a correct immunoregulation of a successful pregnancy. It is also well known that many pathologies associated to infertility are related to oxidative stress. In this paper we analyze membrane fluidity in physiological or oxidative conditions. The ligand–receptor interactions might be modified by oxidative stress; this is the reason to use PIBF–PIBF-R as a good approach to investigate the immunomodulatory disruption that may appear in many infertility pathologies.

Our data indicate that under oxidative stress conditions and in the presence of PIBF: 1) less PIBF is bound to the membrane receptor and 2) raft formation, or clustering is impaired. Both may be responsible for the altered cellular response and failure in immunomodulation during pregnancy. These data together suggest that the failure in PIBF binding to its receptor, thus inhibiting or inactivating signal transduction pathways, may disturb cellular function. A detailed study of plasma membrane lipid dynamics is essential to understand cell function in deleterious oxidative conditions. Further investigation should be performed correlating the modifications in membrane lipid dynamics and their influence on cellular signaling pathways.

Acknowledgements

We are grateful to the Servei de Microscòpia from the Universitat Autònoma de Barcelona (UAB) and the Universitat de Barcelona (UB). We acknowledge Pau Coma for his help in adapting the software to the GP image processing. C.H. was funded with a pre-doctoral fellowship from the UAB. This work was supported by a grant from the Network of Excellence LSHM-CT-2004-512040 (EMBIC) to P.M. and a grant from the Hungarian National Research Fund (OTKA 77717) to J.S-K.

References

[1] J. Szekeres-Bartho, B. Polgar, PIBF: the double edged sword. Pregnancy and tumor, Am. J. Reprod. Immunol. 64 (2010) 77–86.
[2] M.B. Prados, J. La Blunda, J. Szekeres-Bartho, J. Caramelo, S. Miranda, Progesterone induces a switch in oligosaccharyltransferase isoform expression: consequences on IgG N-glycosylation, Immunol. Lett. 137 (2011) 28–37.
[3] J. Szekeres-Bartho, Immunological relationship between the mother and the fetus, Int. Rev. Immunol. 21 (2002) 471–495.

[4] N. Kozma, M. Halasz, B. Polgar, T.G. Poehlmann, U.R. Markert, T. Palkovics, M. Keszei, G. Par, K. Kiss, J. Szeberenyi, L. Grama, J. Szekeres-Bartho, Progesterone-induced blocking factor activates STAT6 via binding to a novel IL-4 receptor, J. Immunol. 176 (2006) 819–826.
[5] K. Gaus, E. Chklovskaia, B. Fazekas de St, W. Groth, W. Jessup, T. Harder, Condensation of the plasma membrane at the site of T lymphocyte activation, J. Cell Biol. 171 (2005) 121–131.
[6] U. Coskun, K. Simons, Membrane rafting: from apical sorting to phase segregation, FEBS Lett. 584 (2010) 1685–1693.
[7] L.J. Pike, The challenge of lipid rafts, J. Lipid Res. 50 (2009) S323–S328, (Suppl.).
[8] K. Jacobson, O.G. Mouritsen, R.G. Anderson, Lipid rafts: at a crossroad between cell biology and physics, Nat. Cell Biol. 9 (2007) 7–14.
[9] A. Catala, Lipid peroxidation of membrane phospholipids generates hydroxy-alkenals and oxidized phospholipids active in physiological and/or pathological conditions, Chem. Phys. Lipids 157 (2009) 1–11.
[10] A. Catala, Lipid peroxidation modifies the picture of membranes from the "Fluid Mosaic Model" to the "Lipid Whisker Model", Biochimie 94 (2012) 101–109.
[11] S. Filosto, E.M. Khan, E. Tognon, C. Becker, M. Ashfaq, T. Ravid, T. Goldkorn, EGF receptor exposed to oxidative stress acquires abnormal phosphorylation and aberrant activated conformation that impairs canonical dimerization, PLoS One 6 (2011) e23240.
[12] M. Almeida, E. Ambrogini, L. Han, S.C. Manolagas, R.L. Jilka, Increased lipid oxidation causes oxidative stress, increased peroxisome proliferator-activated receptor-gamma expression, and diminished pro-osteogenic Wnt signaling in the skeleton, J. Biol. Chem. 284 (2009) 27438–27448.
[13] P.V. Escriba, P.B. Wedegaertner, F.M. Goni, O. Vogler, Lipid–protein interactions in GPCR-associated signaling, Biochim. Biophys. Acta 1768 (2007) 836–852.
[14] J.A. Lundbaek, Regulation of membrane protein function by lipid bilayer elasticity—a single molecule technology to measure the bilayer properties experienced by an embedded protein, J. Phys. Condens. Matter 18 (2006) S1305–S1344.
[15] T.S. Tillman, M. Cascio, Effects of membrane lipids on ion channel structure and function, Cell Biochem. Biophys. 38 (2003) 161–190.
[16] U. Coskun, K. Simons, Cell membranes: the lipid perspective, Structure 19 (2011) 1543–1548.
[17] P. Kaplan, M. Doval, Z. Majerova, J. Lehotsky, P. Racay, Iron-induced lipid peroxidation and protein modification in endoplasmic reticulum membranes. Protection by stobadine, Int. J. Biochem. Cell Biol. 32 (2000) 539–547.
[18] R. Solans, C. Motta, R. Sola, A.E. La Ville, J. Lima, P. Simeon, N. Montella, L. Armadans-Gil, V. Fonollosa, M. Vilardell, Abnormalities of erythrocyte membrane fluidity, lipid composition, and lipid peroxidation in systemic sclerosis: evidence of free radical-mediated injury, Arthritis Rheum. 43 (2000) 894–900.
[19] M. Benderitter, L. Vincent-Genod, J.P. Pouget, P. Voisin, The cell membrane as a biosensor of oxidative stress induced by radiation exposure: a multiparameter investigation, Radiat. Res. 159 (2003) 471–483.
[20] C. de la Haba, J.R. Palacio, P. Martinez, A. Morros, Effect of oxidative stress on plasma membrane fluidity of THP-1 induced macrophages, Biochim. Biophys. Acta 1828 (2012) 357–364.
[21] P.J. Ferret, E. Soum, O. Negre, E.E. Wollman, D. Fradelizi, Protective effect of thioredoxin upon NO-mediated cell injury in THP1 monocytic human cells, Biochem. J. 346 (Pt 3) (2000) 759–765.
[22] Y. Okada, H. Sakai, E. Kohiki, E. Suga, Y. Yanagisawa, K. Tanaka, S. Hadano, H. Osuga, J.E. Ikeda, A dopamine D4 receptor antagonist attenuates ischemia-induced neuronal cell damage via upregulation of neuronal apoptosis inhibitory protein, J. Cereb. Blood Flow Metab. 25 (2005) 794–806.
[23] C.M. Farber, L.F. Liebes, D.N. Kanganis, R. Silber, Human B lymphocytes show greater susceptibility to H2O2 toxicity than T lymphocytes, J. Immunol. 132 (1984) 2543–2546.
[24] W. Han, T. Takano, J. He, J. Ding, S. Gao, C. Noda, S. Yanagi, H. Yamamura, Role of BLNK in oxidative stress signaling in B cells, Antioxid. Redox Signal. 3 (2001) 1065–1073.
[25] D.M. Owen, K. Gaus, A.I. Magee, M. Cebecauer, Dynamic organization of lymphocyte plasma membrane: lessons from advanced imaging methods, Immunology 131 (2010) 1–8.
[26] D. Marguet, P.F. Lenne, H. Rigneault, H.T. He, Dynamics in the plasma membrane: how to combine fluidity and order, EMBO J. 25 (2006) 3446–3457.
[27] T. Parasassi, E. Gratton, W.M. Yu, P. Wilson, M. Levi, Two-photon fluorescence microscopy of laurdan generalized polarization domains in model and natural membranes, Biophys. J. 72 (1997) 2413–2429.
[28] L.A. Bagatolli, To see or not to see: lateral organization of biological membranes and fluorescence microscopy, Biochim. Biophys. Acta 1758 (2006) 1541–1556.
[29] L.A. Bagatolli, E. Gratton, Two photon fluorescence microscopy of coexisting lipid domains in giant unilamellar vesicles of binary phospholipid mixtures, Biophys. J. 78 (2000) 290–305.
[30] L.A. Bagatolli, E. Gratton, Two-photon fluorescence microscopy observation of shape changes at the phase transition in phospholipid giant unilamellar vesicles, Biophys. J. 77 (1999) 2090–2101.
[31] L.A. Bagatolli, S.A. Sanchez, T. Hazlett, E. Gratton, Giant vesicles, laurdan, and two-photon fluorescence microscopy: evidence of lipid lateral separation in bilayers, Methods Enzymol. 360 (2003) 481–500.
[32] K. Gaus, S. Le Lay, N. Balasubramanian, M.A. Schwartz, Integrin-mediated adhesion regulates membrane order, J. Cell Biol. 174 (2006) 725–734.
[33] W. Yu, P.T. So, T. French, E. Gratton, Fluorescence generalized polarization of cell membranes: a two-photon scanning microscopy approach, Biophys. J. 70 (1996) 626–636.
[34] A. Stacchini, M. Aragno, A. Vallario, A. Alfarano, P. Circosta, D. Gottardi, A. Faldella, G. Rege-Cambrin, U. Thunberg, K. Nilsson, F. Caligaris-Cappio, MEC1 and MEC2: two new cell lines derived from B-chronic lymphocytic leukaemia in prolymphocytoid transformation, Leuk. Res. 23 (1999) 127–136.
[35] K. Gaus, T. Zech, T. Harder, Visualizing membrane microdomains by Laurdan 2-photon microscopy, Mol. Membr. Biol. 23 (2006) 41–48.
[36] K. Gaus, E. Gratton, E.P. Kable, A.S. Jones, I. Gelissen, L. Kritharides, W. Jessup, Visualizing lipid structure and raft domains in living cells with two-photon microscopy, Proc. Natl. Acad. Sci. U. S. A. 100 (2003) 15554–15559.
[37] E.H. Pap, G.P. Drummen, V.J. Winter, T.W. Kooij, P. Rijken, K.W. Wirtz, J.A. Op den Kamp, W.J. Hage, J.A. Post, Ratio-fluorescence microscopy of lipid oxidation in living cells using C11-BODIPY(581/591), FEBS Lett. 453 (1999) 278–282.
[38] G.P. Drummen, L.C. van Liebergen, J.A. Op den Kamp, J.A. Post, C11-BODIPY(581/591), an oxidation-sensitive fluorescent lipid peroxidation probe: (micro) spectroscopic characterization and validation of methodology, Free Radic. Biol. Med. 33 (2002) 473–490.
[39] E.H. Pap, G.P. Drummen, J.A. Post, P.J. Rijken, K.W. Wirtz, Fluorescent fatty acid to monitor reactive oxygen in single cells, Methods Enzymol. 319 (2000) 603–612.
[40] E. Niki, Free radical initiators as source of water- or lipid-soluble peroxyl radicals, Methods Enzymol. 186 (1990) 100–108.
[41] E. Schnitzer, I. Pinchuk, D. Lichtenberg, Peroxidation of liposomal lipids, Eur. Biophys. J. 36 (2007) 499–515.
[42] C. Dietrich, L.A. Bagatolli, Z.N. Volovyk, N.L. Thompson, M. Levi, K. Jacobson, E. Gratton, Lipid rafts reconstituted in model membranes, Biophys. J. 80 (2001) 1417–1428.
[43] L.A. Bagatolli, T. Parasassi, E. Gratton, Giant phospholipid vesicles: comparison among the whole lipid sample characteristics using different preparation methods: a two photon fluorescence microscopy study, Chem. Phys. Lipids 105 (2000) 135–147.
[44] B. Yang, T.N. Oo, V. Rizzo, Lipid rafts mediate H2O2 prosurvival effects in cultured endothelial cells, FASEB J. 20 (2006) 1501–1503.
[45] K.S. George, S. Wu, Lipid raft: A floating island of death or survival, Toxicol. Appl. Pharmacol. 259 (2011) 311–319.
[46] S.P. Lu, M.H. Lin Feng, H.L. Huang, Y.C. Huang, W.I. Tsou, M.Z. Lai, Reactive oxygen species promote raft formation in T lymphocytes, Free Radic. Biol. Med. 42 (2007) 936–944.
[47] J. Cuschieri, S. Sakr, E. Bulger, M. Knoll, S. Arbabi, R.V. Maier, Oxidant alterations in CD16 expression are cytoskeletal induced, Shock 32 (2009) 572–577.
[48] P.F. Almeida, A. Pokorny, A. Hinderliter, Thermodynamics of membrane domains, Biochim. Biophys. Acta 1720 (2005) 1–13.
[49] K. Jacobson, C. Dietrich, Looking at lipid rafts? Trends Cell Biol. 9 (1999) 87–91.
[50] A. Larbi, N. Douziech, G. Dupuis, A. Khalil, H. Pelletier, K.P. Guerard, T. Fulop Jr., Age-associated alterations in the recruitment of signal-transduction proteins to lipid rafts in human T lymphocytes, J. Leukoc. Biol. 75 (2004) 373–381.
[51] A. Kusumi, I. Koyama-Honda, K. Suzuki, Molecular dynamics and interactions for creation of stimulation-induced stabilized rafts from small unstable steady-state rafts, Traffic 5 (2004) 213–230.
[52] K. Simons, D. Toomre, Lipid rafts and signal transduction, Nat. Rev. Mol. Cell Biol. 1 (2000) 31–39.
[53] M. Kulma, K. Kwiatkowska, A. Sobota, Raft coalescence and FcgammaRIIA activation upon sphingomyelin clustering induced by lysenin, Cell. Signal. 24 (2012) 1641–1647.
[54] E. Altrock, C.A. Muth, G. Klein, J.P. Spatz, C. Lee-Thedieck, The significance of integrin ligand nanopatterning on lipid raft clustering in hematopoietic stem cells, Biomaterials 33 (2012) 3107–3118.
[55] B.D. Rockett, H. Teague, M. Harris, M. Melton, J. Williams, S.R. Wassall, S.R. Shaikh, Fish oil increases raft size and membrane order of B cells accompanied by differential effects on function, J. Lipid Res. 53 (2012) 674–685.
[56] F.M. Goni, A. Alonso, Effects of ceramide and other simple sphingolipids on membrane lateral structure, Biochim. Biophys. Acta 1788 (2009) 169–177.
[57] S.N. Pinto, F. Fernandes, A. Fedorov, A.H. Futerman, L.C. Silva, M. Prieto, A combined fluorescence spectroscopy, confocal and 2-photon microscopy approach to re-evaluate the properties of sphingolipid domains, Biochim. Biophys. Acta 1828 (2013) 2099–2110.
[58] E. Gulbins, S. Dreschers, B. Wilker, H. Grassme, Ceramide, membrane rafts and infections, J. Mol. Med. (Berl) 82 (2004) 357–363.
[59] L.C. Silva, R.F. de Almeida, B.M. Castro, A. Fedorov, M. Prieto, Ceramide-domain formation and collapse in lipid rafts: membrane reorganization by an apoptotic lipid, Biophys. J. 92 (2007) 502–516.
[60] B.M. Castro, L.C. Silva, A. Fedorov, R.F. de Almeida, M. Prieto, Cholesterol-rich fluid membranes solubilize ceramide domains: implications for the structure and dynamics of mammalian intracellular and plasma membranes, J. Biol. Chem. 284 (2009) 22978–22987.
[61] J.M. Denu, K.G. Tanner, Specific and reversible inactivation of protein tyrosine phosphatases by hydrogen peroxide: evidence for a sulfenic acid intermediate and implications for redox regulation, Biochemistry 37 (1998) 5633–5642.
[62] J.H. Check, E. Levin, A. Bollendorf, J. Locuniak, Miscarriage in the first trimester according to the presence or absence of the progesterone-induced blocking factor at three to five weeks from conception in progesterone supplemented women, Clin. Exp. Obstet. Gynecol. 32 (2005) 13–14.
[63] J. Szekeres-Bartho, G. Szekeres, P. Debre, B. Autran, G. Chaouat, Reactivity of lymphocytes to a progesterone receptor-specific monoclonal antibody, Cell. Immunol. 125 (1990) 273–283.
[64] B. Polgar, A. Barakonyi, I. Xynos, J. Szekeres-Bartho, The role of gamma/delta T cell receptor positive cells in pregnancy, Am. J. Reprod. Immunol. 41 (1999) 239–244.
[65] J. Szekeres-Bartho, A. Barakonyi, B. Polgar, G. Par, Z. Faust, T. Palkovics, L. Szereday, The role of gamma/delta T cells in progesterone-mediated immunomodulation during pregnancy: a review, Am. J. Reprod. Immunol. 42 (1999) 44–48.

[66] K. Kelemen, I. Bognar, M. Paal, J. Szekeres-Bartho, A progesterone-induced protein increases the synthesis of asymmetric antibodies, Cell. Immunol. 167 (1996) 129–134.
[67] M. Halász, At the Crossroad of Physiological and Pathological Invasion: The Role of Progesterone-Induced Blocking Factor in Trophoblast and Tumor Invasion. (PhD Thesis) University of Pécs, Pécs (Hungary), 2011.
[68] I. Hudic, J. Szekeres-Bartho, Z. Fatusic, B. Stray-Pedersen, L. Dizdarevic-Hudic, A. Latifagic, N. Hotic, L. Kameric, A. Mandzic, Dydrogesterone supplementation in women with threatened preterm delivery—the impact on cytokine profile, hormone profile, and progesterone-induced blocking factor, J. Reprod. Immunol. 92 (2010) 103–107.